ALMA Memo 456

Characteristics of a reflector antenna

Parameters, graphs and formulae for Cassegrain systems with Mathematica expressions for numerical computation

Jacob W.M. Baars
ESO / NRAO, Tucson AZ
April 2003

Keywords: Antenna theory, Cassegrain antenna, Radio telescope, Reflector antenna, Mathematica

Summary. In this report I collect data on the characteristics of a reflector antenna in the form of Figures and Formulae. The goal is to make available in one place information which is useful for the analysis of antenna measurements and radio astronomy observations. I discuss the illumination efficiency, axial and lateral defocus, pointing aspects, aperture blocking and random surface errors. The computations and the derived illustrations are made with the aid of *Mathematica* and all *Mathematica* expressions are included at the end of the report. This collection of data is an extension of my earlier summary of antenna parameters, issued as an NRAO Electronic Division Internal Report (EDIR), No.57 of August 1966. Some of the figures of that report are included here.

Contents Page

1. Introduction

The paraboloidal reflector antenna, in the configuration with a primary focus feed or a secondary reflector in the Cassegrain or Gregorian geometry, is the most widely used form of radio telescope, either as an independent single antenna or as element of an interferometric array. For the characterization of such antennas, often done by means of radio astronomical measurements, it is convenient to have formulae, curves and tables of its major parameters readily available. It is the purpose of this Report to provide those. The impetus for collecting the following material was the need to evaluate the two ALMA prototype antennas in a unified way. Therefore, all numerical examples below are applicable to the geometry of the ALMA Cassegrain antennas. The formulas are presented in a general form, so other starting parameters can readily be inserted. In addition, the equations are presented in the form of *Mathematica* expressions. After inserting the applicable variable range or starting parameters, these expressions can be run with *Mathematica* to provide data for other antenna configurations.

A number of useful figures are included with data which were obtained from outside sources, for which *Mathematica* expressions could not readily be constructed. Some of these are derived from calculations performed by me (see Baars, Dissertation 1970) and were earlier contained in the NRAO Electronic Division Internal Report (EDIR), No. 57, August 1966. Actually, the current report could be considered an expanded version of that earlier report.

The material is presented in its final form without complete derivation. The purpose of the report is to be of use in actual practice, not to present a coherent theory of the antenna's characteristics. References are only given, where they appear to be useful and are by no means exhaustive.

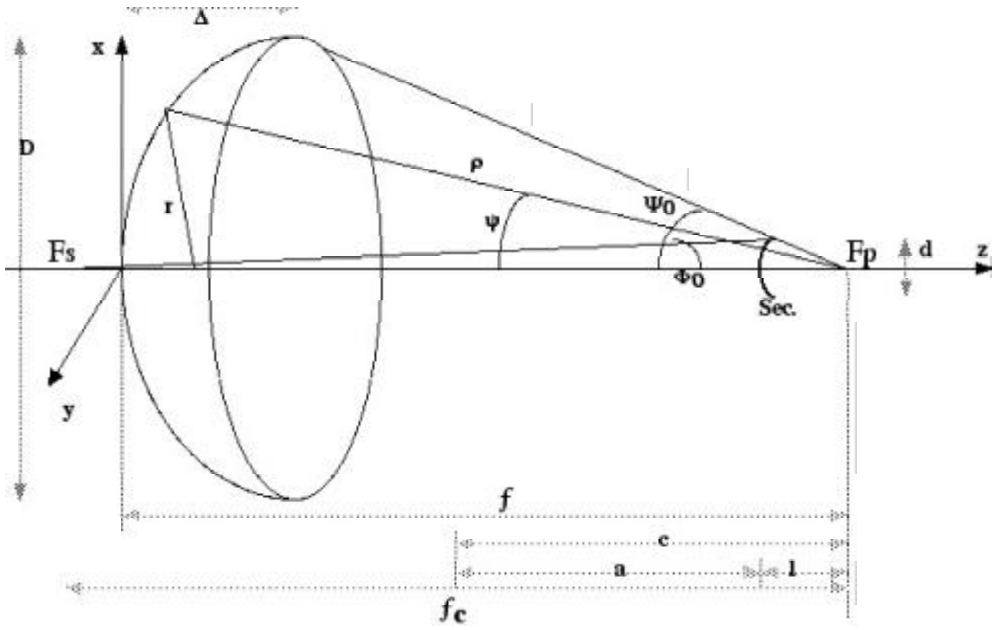

Fig. 1. - Geometry of the Cassegrain reflector antenna

2. Geometry of Cassegrain antenna

The primary reflector is assumed to be a "classical" paraboloid, while the secondary mirror in a Cassegrain system has the shape of a hyperboloid. The Gregorian system applies an elliptic secondary. It is not widely used, the major exponent of this geometry is the Effelsberg 100-m radio telescope. Referring to Fig.1 for the meaning of the variables, the equations for these reflectors can be written as follows:

paraboloid	$\rho = 2f / (1 + \cos\psi) = f \sec^2(\psi/2)$	in spherical coordinates
	$r^2 = x^2 + y^2 = 4fz$	in cartesian coordinates
hyperboloid	$r_s = (c^2 - a^2) / (a + c\cos\psi)$	in spherical coordinates
ellipsoid	$r_s = (c^2 - a^2) / (c - a\cos\psi)$	in spherical coordinates

An alternative expression, easily derived from the first equation above, for the paraboloid is

$$\tan(\psi/2) = \frac{r}{2f}$$

from which follows

$$\tan(\Psi_0/2) = \frac{D}{4f}\ , \qquad (1)$$

where D is the diameter, Ψ_0 the opening half-angle of the reflector and f its focal length.
The "depth" Δ of the paraboloid is given by

$$\Delta = \frac{D^2}{16f} = f\left(\frac{D}{4f}\right)^2 = f\left(\tan\frac{\Psi_0}{2}\right)^2. \qquad (2)$$

The Cassegrain system is characterised by the ***magnification factor*** **m**, connected to the ***eccentricity e*** of the hyperboloidal secondary by the relations

$$m = (e+1)/(e-1) \quad \text{or} \tag{3a}$$
$$e = (m+1)/(m-1) \tag{3b}$$

The "equivalent paraboloid" of the Cassegrain antenna is given by

$$\tan(\varphi/2) = \frac{r}{2mf},$$

from which follows

$$\tan(\Phi_0/2) = \frac{D}{4mf}, \tag{4}$$

where Φ_0 is the opening half-angle of the secondary reflector from the Cassegrain focus. Hence we have

$$m = \tan(\Psi_0/2)/\tan(\Phi_0/2). \tag{5}$$

Further

$$c = \frac{d}{4}(\cot\Psi_0 + \cot\Phi_0), \tag{6}$$

where c is the "focal length" and d the diameter of the hyperboloid. The distance between primary and secondary focus of the Cassegrain system is $f_c = 2c$ and the distance from primary focus to secondary vertex is $l = c - a$ (see Fig.1). We have the relations

$$f_c = 2c \tag{7a}$$
$$l \equiv c - a = c(e-1)/e \tag{7b}$$
$$a = c/e = c(m-1)/(m+1) \tag{7c}$$

In the special case where the secondary focus coincides with the vertex of the primary (i.e. $f_c = f$), we have the situation that Eq.(4) can be written as $\tan(\Phi_0/2) = d/(4f)$, leading to the simple expression $\mathbf{m = D/d}$.
For use in numerical calculations with *Mathematica*, we list the equations in **Input** format in Section 7 of this Report. The examples for the input variables are mostly taken from the 12-m ALMA prototype antennas.

3. Aperture and illumination efficiency

■ 3.1. Definition of aperture efficiency and its components

The aperture efficiency is a basic parameter defining the sensitivity of the antenna. It is determined by a number of phenomena and hence it can be seen as the product of a number of separate "efficiency components". We consider a reflector antenna with an unambiguously defined geometrical aperture area A_g, which in the case of a circular aperture is $A_g = \pi D^2/4$, where D is the diameter of the aperture. The fundamental number for expressing the sensitivity of the antenna is the **effective** aperture area A_e, sometimes called *absorption area*. Normally, the sensitivity is expressed as the ***aperture efficiency***, which is defined as

$$\eta_a = A_e/A_g\,. \tag{8}$$

Following, for instance, Kraus, Radio Astronomy, Chapter 6.25b (page 6-110), we can write the aperture efficiency as the product of a number of individual components:

$$\eta_a = \eta_i \eta_s \eta_r \eta_p \eta_e \eta_f \eta_b , \qquad (9)$$

where η_i = illumination efficiency of the aperture by the feed function ("taper")
η_s = spillover efficiency of the feed (and subreflector, if present)
η_r = radiation efficiency of the reflector surface (ohmic loss)
η_p = polarization efficiency of the feed-reflector combination
η_e = surface error efficiency ("Ruze loss"), also called scattering efficiency
η_f = focus error efficiency (both radial and axial defocus)
η_b = blocking efficiency due to quadripod, subreflector and possible other obstruction.

It is important to note here that by this definition all components of the final aperture efficiency are related to the geometrical area of the reflector aperture. In other words, each of them reduces the aperture area by an amount proportional to the individual efficiency magnitude.

Let us look at the different components in some more detail.
- taper: the taper is chosen to reduce the nearby sidelobes and the spillover. Thus there is a relation between the illumination and spillover efficiency. The detailed choice depends on the required sidelobe level, the ratio of receiver temperature to the expected spillover contribution (which will be different for Cassegrain and prime focus systems) and the acceptable beam broadening and loss of sensitivity. Often a maximization of the ratio A_e / T_s is the goal, where T_s is the overall system temperature, which contains a spillover contribution.

- spillover: as remarked above, the spillover is directly related to the edge taper of the illumination function. The received spillover power is dependent on whether the "spilled" radiation comes mainly from the warm ground (prime focus) or cool sky (Cassegrain). It is also dependent on the elevation angle.

- ohmic loss: with a metallic reflector this factor is close to one, but at very high frequencies (submm wavelengths) and/or with a paint layer on the reflector, the losses may become significant (several percent).

-polarization: the loss due to cross-polarization is mainly dependent on the feed design, although some of it can be caused by the curved reflectors. It is often the least known factor, because it is not easy to calculate and difficult to measure accurately.

- surface errors: the small scale, randomly distributed deviations of the reflector from the prescribed (paraboloidal) shape cause randomly distributed phase errors over the aperture. Their effect has been analyzed by Ruze and resulted in the well known "Ruze formula" for the efficiency loss due to these errors. Strictly speaking, the Ruze analysis is valid only in case the correlation length of the surface errors is much larger than the wavelength and much smaller than the reflector diameter. In practice, however, this requirement appears to be rather flexible.

- focus: axial or radial displacements of the feed from the focus cause large scale, systematic phase errors over the aperture, which normally are amenable to calculation. One tries to minimize these errors by (regular) determination of the optimum focus from test observations.

- blocking: the central subreflector and its support structure cause a partial shadowing of the aperture, which leads to a loss of efficiency. The blocking area consists normally of two parts: the "plane wave blocking", equal to the projection of the structure onto the aperture plane, and the "spherical wave blocking", which is the shadow cast by the spherical waves traveling form the outer region of the reflector (outside the support penetration point) to the focus. Only if the support is attached at the rim of the main reflector (e.g. BIMA) will the spherical blocking component vanish.

■ 3.2. Discussion

The illumination function of the aperture, determined by the feed radiation pattern, has a special significance. It determines the degree to which the outer areas of the aperture are less effectively exploited as a result of the "weaker" illumination of that area. Consequently, other errors which are distributed over the aperture will have a reduced influence on the aperture efficiency to the extent that they are diminished by the smaller illumination intensity in the outer aperture area. Their influence on the overall efficiency is "weighted" by the illumination function at the location where their effect occurs. For a realistic evaluation of the overall aperture efficiency such a weighting is admissible. For instance, it is well known that the influence of the generally larger reflector deformations towards the edge of the reflector is diminished by the smaller illumination level and hence gives a reduced contribution to the "Ruze loss". Similarly, we can weigh the blocking areas with the illumination function, which will yield a smaller effective blocking area. It should be noted that, after having applied the weighting, where applicable, and having computed the effective loss in aperture, in order to correctly introduce this in the efficiency formula, it must be treated as a loss of area compared to the geometrical aperture area of the real reflector.

Sometimes the concept of the "tapered reflector radius" is applied (e.g. by Mangum and Cheng in MMA Memo 197, Feb.1998), which is defined as the radius of a uniformly illuminated reflector with the same effective area as the real reflector with a tapered illumination. The "tapered radius" is useful in that it will give a quick indication of the "loss" of actually fabricated reflector area due to the tapered illumination. It is, however, not allowed to use the "tapered reflector radius" in the calculation of the components of the aperture efficiency. Based on the definition of aperture efficiency above, the different efficiency components must all be referenced to the full geometrical aperture area in order to arrive at the correct value of the overall aperture efficiency. Introducing a "tapered reflector" for some of those efficiency components is not admissible, because the illumination efficiency already has accounted for it.

■ 3.3. Illumination efficiency ("taper")

The illumination function of the aperture $F(r, \varphi)$ is equivalent, but not identical, to the radiation pattern of the feed in the focal point. This function determines the illumination efficiency of the antenna, which is the ratio of the gain of the antenna to that of a uniformly illuminated aperture. The illumination function is normally characterized by the "edge taper", i.e. the level of the illumination at the edge of the reflector compared to that in the center. However, different functional forms of the illumination function with the same edge level can result in different values for the illumination efficiency.

The level of the feed function at the opening angle of the reflector is further reduced by the "free-space taper", determined by the path length difference between the edge and central rays. The free-space taper T_f (in dB) is dependent on the focal ratio and is given by the expression (and shown in Fig.2)

$$T_f = 20 \log\left(\left(\sec \tfrac{\Psi_0}{2}\right)^2\right) \equiv 20 \log\left(1 + \left(\tfrac{D}{4f}\right)^2\right). \qquad (10)$$

The **illumination efficiency** η_i is defined (see e.g. Silver, 1947) by the following equation:

$$\eta_i = \frac{\{\int F(r,\varphi)\, dA\}^2}{\int F^2(r,\varphi)\, dA}, \qquad (11)$$

where the integration is extended over the aperture. We consider circularly symmetric amplitude illumination functions with constant phase front. Thus thee integration over φ is trivial and the integration over r can be carried

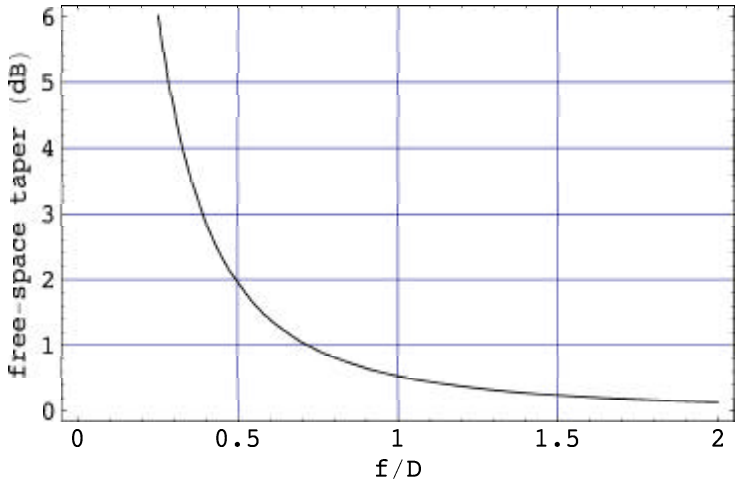

Fig.2. The free-space taper in dB as function of the focal ratio of the reflector.

out in closed form for suitably chosen functions F(r). Here follow the results for two widely applied illumination functions, each with a freely chosen value of the level at the aperture edge, the edge taper T_e in dB. Note that this value includes the free-space taper.

i) the gaussian distribution with an edge taper T_e (in dB), is expressed by

$$F(r) = \exp\{-\alpha (r/r_0)^2\} \tag{12}$$

where r_0 is the aperture radius and $\alpha = (T_e/20)\ln(10)$. For T_e= 11 dB, we have α = 1.2664. Substituting Eq.(12) into Eq.(11) and performing the integration yields

$$\eta_i = \frac{2(1-e^{-\alpha})^2}{\alpha(1-e^{-2\alpha})}, \tag{13}$$

which for the selected taper of 11 dB delivers an illumination efficiency $\eta_i = 0.885$.

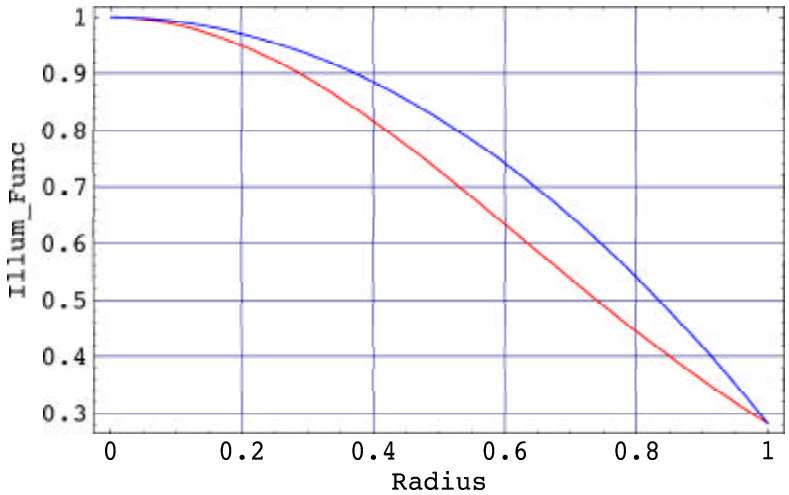

Fig.3. The illumination function for the gaussian (red, lower curve) and parabolic (blue, upper) distribution and an edge taper of 11 dB. The parabolic illumination is slightly more effective.

ii) the parabolic on a pedestal distribution, with an edge level τ and normalised to one in the aperture center, is given by

$$F(r) = \tau + (1-\tau)\{1-(r/r_0)^2\} \equiv 1-(1-\tau)(r/r_0)^2. \qquad (14)$$

After substitution into Eq.(11) and carrying out the integration, we obtain

$$\eta_i = \frac{\{1-(1-\tau)/2\}^2}{\tau+(1-\tau)^2/3} = \frac{3(1+\tau)^2}{4(1+\tau+\tau^2)}, \qquad (15)$$

where $\log(\tau) = -T_e/20$, again T_e expressed in dB (see Fig. 4). For $T_e = 11$ dB we find $\eta_i = 0.904$.
This is close to the value for the gaussian distribution, indicating that the illumination functions are rather similar. This is illustrated by drawing the two functions, as shown in Fig.3. The parabolic function lies somewhat above the gaussian one and it results in a slightly higher illumination efficiency. The calculated spill-over efficiencies are 0.95 and 0.75 for the parabolic and gaussian distribution, respectively. This strengthens the argument in favour of the parabolic distribution.

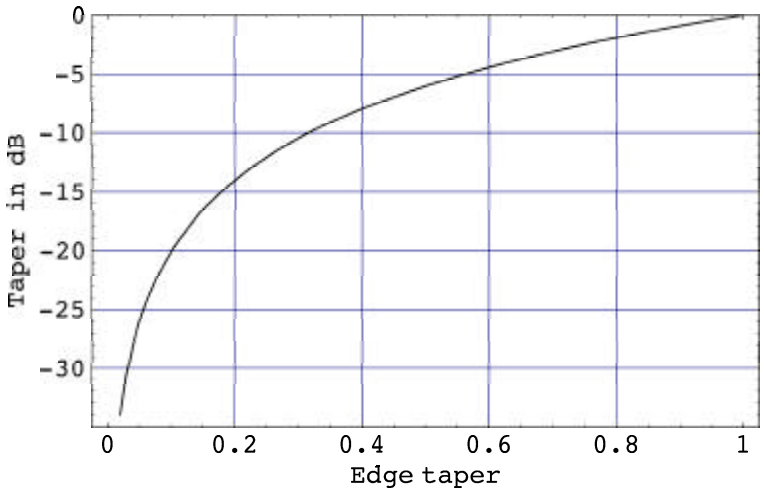

Fig.4. The edge taper in dB against the value of τ for the parabolic illumination function.

Note that the parabolic distribution going to zero at the reflector edge ($\tau = 0$) reduces the illumination efficiency to 0.75 times the maximum value for uniform illumination. For a gaussian illumination with an edge value of about 2%, i.e. $\alpha \approx 4$, the illumination efficiency decreases to about 0.5. Obviously, to maximize the efficiency for a given edge taper, the parabolic distribution is preferable. Indeed, optimized feed horns exhibit a pattern, which is approaching the parabolic function, rather than the often assumed gaussian shape. In Fig.5 we show the two functions of Eqs.(13) and (15) as function of the taper T_e in dB, again indicating the higher efficiency of the parabolic distribution.

Finally, note that these illumination functions implicitly contain the free-space taper. For instance, if the desired aperture taper is 15 dB and the reflector geometry introduces 3 dB of free-space taper, the feed must be designed to have a 12 dB amplitude decrease at the opening angle of the reflector.

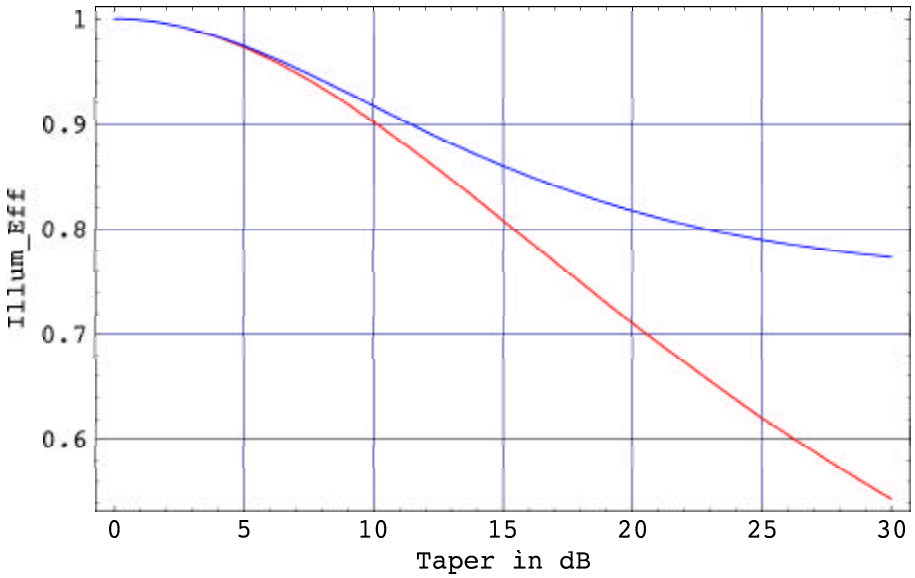

Fig.5. The illumination efficiency as function of the edge taper (in dB) for the gaussian (red, lower curve) and parabolic (blue, upper) distribution. The parabolic illumination is more effective.

■ 3.4. Beamwidth, sidelobe level and taper

The normalised radiation function for the parabolic on a pedestal illumination function (Eq.14) of constant phase takes the form

$$f(u) = \int_0^1 F(r)\, J_0(u\, r)\, r\, dr,$$

where $J_0(u\, r)$is the Bessel function of the first kind and order zero. Integration over r yields

$$\boldsymbol{f(u) = \tau\, \Lambda_1(u) + (1-\tau)\, \frac{\Lambda_2(u)}{2}}, \qquad (16)$$

where the Lambda function is defined as $\Lambda_n(u) = n!\, \frac{J_n(u)}{(u/2)^n}$, with $J_n(u)$ the Bessel function of the first kind and order n. The angular coordinate $u = (\pi D/\lambda)\sin(\theta)$. The Lambda functions are tabulated in Jahnke-Emde's "Tables of Functions", p.180ff (Dover Books). Thus, for uniform illumination (τ=1) we obtain the Lambda function of order one, while for full parabolic illumination (τ=0) the pattern is given by the Lambda function of order two. The **"power pattern" (also called gain function)** $\boldsymbol{g(u)}$ of the antenna is the square of the function $f(u)$. Written in Bessel functions, the power pattern becomes

$$\boldsymbol{g(u) = \left(2\,\tau\, \frac{J_1(u)}{u} + 4\,(1-\tau)\, \frac{J_2(u)}{u^2}\right)^2}. \qquad (17)$$

These are directly available in *Mathematica*. The following figure illustrates the function $g(u)$ for values τ =(0, step 0.2, 1). We have normalised all curves to one to improve the visibility of the differences. The narrowest curve pertains to the uniform illumination, the broadest to the parabolic illumination with edge level zero.

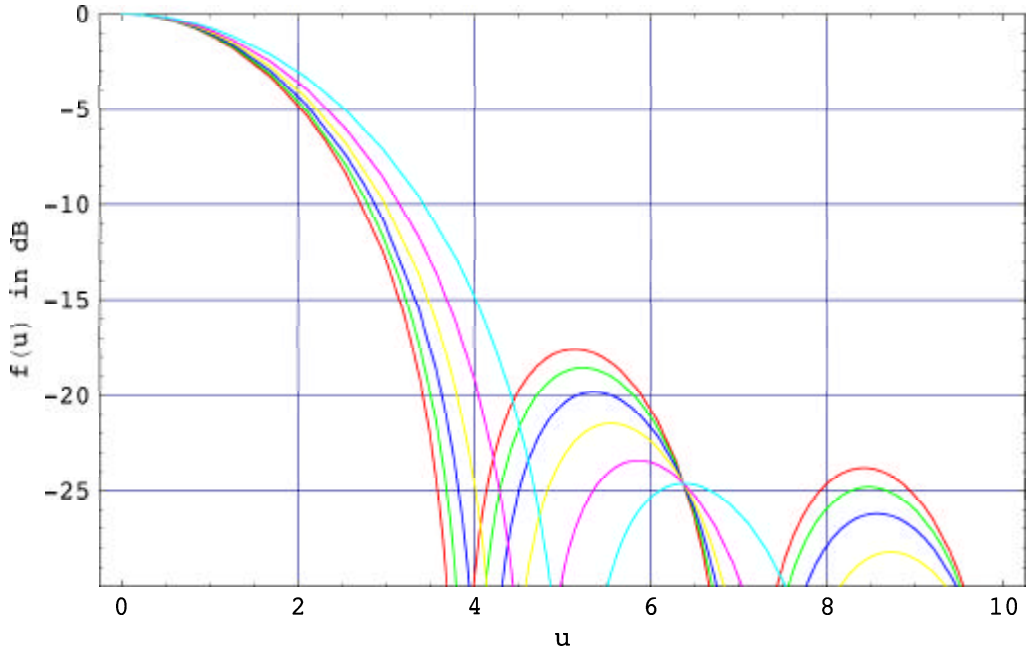

Fig.6. Power pattern of a circular aperture with parabolic illumination function and edge taper values of 1, 0.8, 0.6, 0.4, 0.2 and 0, from left to right.

We can use these results to obtain a curve of the half power beam width (HPBW) as function of the illumination taper τ. This is illustrated in Fig. 7, which shows the factor **b** in the expression for the HPBW: $\Theta_A = \mathbf{b}\ (\lambda/\mathbf{D})$. The range $0.1<\tau<1$ can be approximated very well by the expression

$$b = 1.243 - 0.343\,\tau + 0.12\,\tau^2 \qquad (18)$$

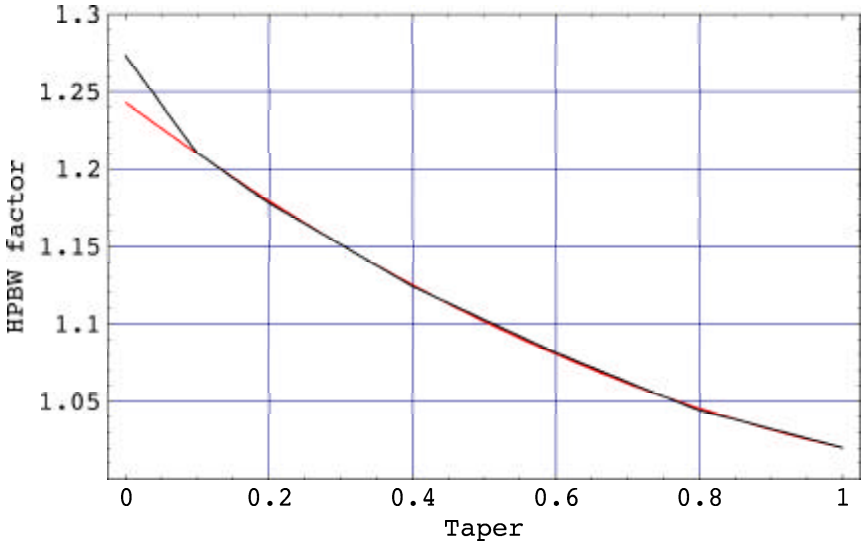

Fig.7. The factor **b** in the HPBW formula as function of the taper τ. The red line is the quadratic approximation of Eq. (18) above.

In Eq.(15) the illumination efficiency was given as function of the taper parameter τ. One could use this expression to derive a "tapered aperture diameter" D_{eff}, defined as the diameter of a uniformly illuminated reflector with the same effective area as the real reflector with tapered illumination. Thus D_{eff} is proportional to the square root of η_i, as given in Eq.(15). Using the effective diameter one can compute the expected change is HPBW from the simple relation that the HPBW is inversely proportional to the diameter of the reflector. The result gives values which are smaller than the HPBW, determined directly from the computed radiation pattern. *The concept of effective diameter seems to have only a limited usefulness in the analysis of the antenna behaviour*.

From the pattern calculations of Fig.6 we can also derive the level of the sidelobes as function of the illumination taper. We see a significant decrease in the level of the first sidelobe if the illumination becomes more tapered, which corresponds to a smaller value of τ (τ = 1 for uniform illumination). Next to the desire to minimise spill-over radiation along the edge of the reflector, the lower sidelobe level is an important factor in choosing a tapered illumination. Fig.8 illustrates the sidelobe level in dB as function of the taper parameter τ. To an accuracy of a few tenths of a decibel over the range $0<\tau<0.8$, the relation can be approximated by the simple formula

$$S(\text{dB}) = -24.7 + 7.9\,\tau\,. \qquad (19)$$

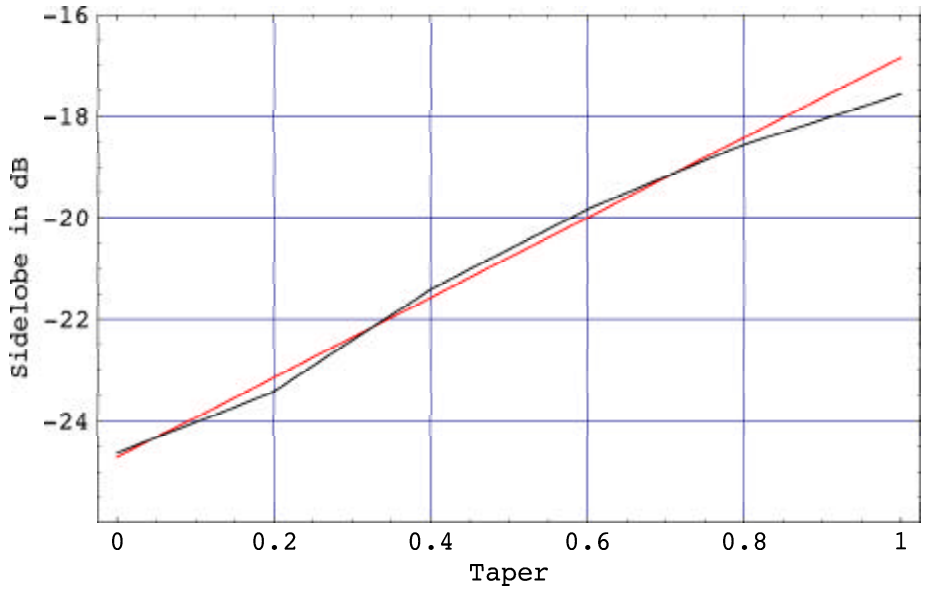

Fig.8. The level of the first sidelobe in dB as function of the taper τ.
The red line is the approximation of the above equation.

4. Out of focus characteristics

■ 4.1. Axial defocus

■ 4.1.1. Depth of focus

It is well known that the large effective focal ratio of the Cassegrain produces a large field of view in the secondary focal plane. Also the "depth of focus" along the axis is increased with respect to the primary focus. Thus placement of the feed in the secondary focus is less critical and multi-feed systems can be accommodated without significant deterioration of the beam for the outer, off-axis feeds. The depth of focus can be illustrated in the following way. (Refer to Fig.1 for the meaning of the angles φ and ψ.) The phase error caused by an axial defocus of the subreflector δ_s is given by

$$\Delta\phi_s = (2\pi/\lambda)(2 - \cos\varphi - \cos\psi)\,\delta_s\,, \tag{20}$$

while that due to an axial defocus of the feed in the secondary focus δ_f is

$$\Delta\phi_f = (2\pi/\lambda)(1 - \cos\varphi)\,\delta_f\,. \tag{21}$$

These relations can be expanded to show that the phase error is proportional to even powers of r.
For an equal phase error over the aperture we obtain the expression

$$\delta_f / \delta_s = 1 + \frac{1-\cos\Psi_0}{1-\cos\Phi_0} = m^2 \frac{1+\tan^2(\Phi_0/2)}{1+m^2\tan^2(\Phi_0/2)}\,. \tag{22}$$

The depth of focus in the secondary is of the order of m^2 times that in the primary focus. Typical values for Φ_0 of a few degrees lead to a numerical value of the second term in Eq.(22) of about 0.7.
The *Mathematica* form of the equation for the focal depth is reproduced in Sec.7.

■ 4.1.2. Gain decrease

The loss of gain, or aperture efficiency, caused by axial defocusing can be computed by integrating the radiation function with the resulting phase error over the aperture. We assume the circularly symmetrical, equiphase, amplitude tapered aperture illumination function of Eq.(14). Adding the phase function of Eq. (21) and introducing this in the radiation integral (just above Eq.(16)), one can integrate this equation while setting u=0 (on axis) to obtain the decrease of amplitude as function of the axial defocus δ. Then, the following expression is obtained for the relative decrease in gain

$$\eta_f \equiv \frac{G}{G_0} = \tau^2 \left(\frac{\sin(\beta/2)}{\beta/2}\right)^2 + (1-\tau^2)\left\{\left(\frac{\sin(\beta/2)}{\beta/2}\right)^4 + \frac{4}{\beta^2}\left(\frac{\sin\beta}{\beta} - 1\right)^2\right\}, \tag{23}$$

where $\beta = (2\pi/\lambda)(1 - \cos\Psi_0)\,\delta$ with the maximum values of Ψ_0 or Φ_0 of Eq. (20) or (21). The case of uniform illumination is represented by the first term with $\tau = 1$. In the *Mathematica* input function we insert the **defocus δ in units of wavelength** to obtain the universal curves of Fig.9. Because the taper τ appears quadratically in Eq.(23), the curves for practical taper values lie very close to the parabolic case.

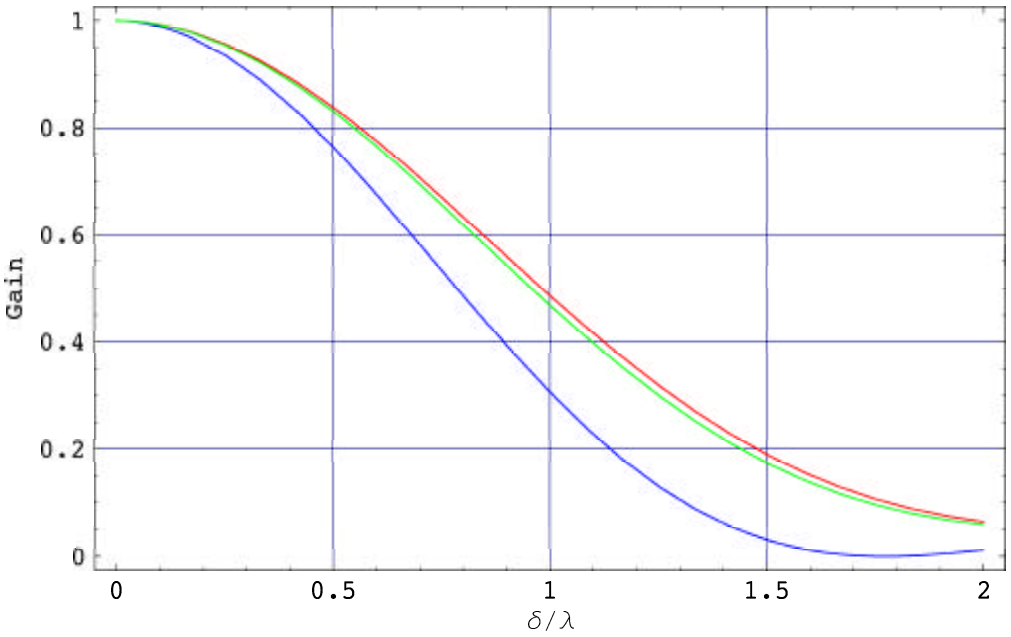

Fig.9. Gain loss as function of axial defocus in units of wavelength. Blue, lower curve: uniform illumination; red, upper parabolic illumination and green for τ=0.25 (-12 dB).

The curves apply to the axial defocusing of the subreflector of a Cassegrain system. By setting cos φ =1 in Eq.(20) we obtain the case for the axial movement of the feed in the primary focus. The axial defocus does not cause a change in the beam direction; hence there are no pointing errors in this case.

4.2. Lateral defocus

4.2.1. Beam Deviation Factor (BDF)

A lateral movement of the feed or subreflector from the focal point will cause a shift of the beam away form the axis; i.e. the antenna exhibits a pointing error. The relationship between the amount of defocus and the pointing shift is called the ***beam deviation factor*** (BDF). It is a number smaller than one and it is caused by the curved shape of the primary reflector, or the equivalent primary in the case of a Cassegrain system. Qualitatively it is easy to see that the BDF will be smaller for a "deeper" reflector, i.e. one with a smaller f/D-ratio. The BDF is also dependent on the illumination function. The functional form of the BDF has been given by Ruze (1965). For a paraboloidal reflector of normalised radius and a ratio $f/D = f^*$ and illumination function $f(r)$, the formula is

$$\text{BDF} = \int_0^1 \frac{f(r)\, r^3}{1+\left(\frac{r}{4f^*}\right)^2} \Big/ \int_0^1 f(r)\, r^3\, dr \qquad (24)$$

For the parabolic on a pedestal illumination function, introduced in Eq.(14), the integration can be tediously performed in closed form. The *Mathematica* integration (see Section 7.4) delivers this result automatically and we present the outcome of the computation in Fig.10.

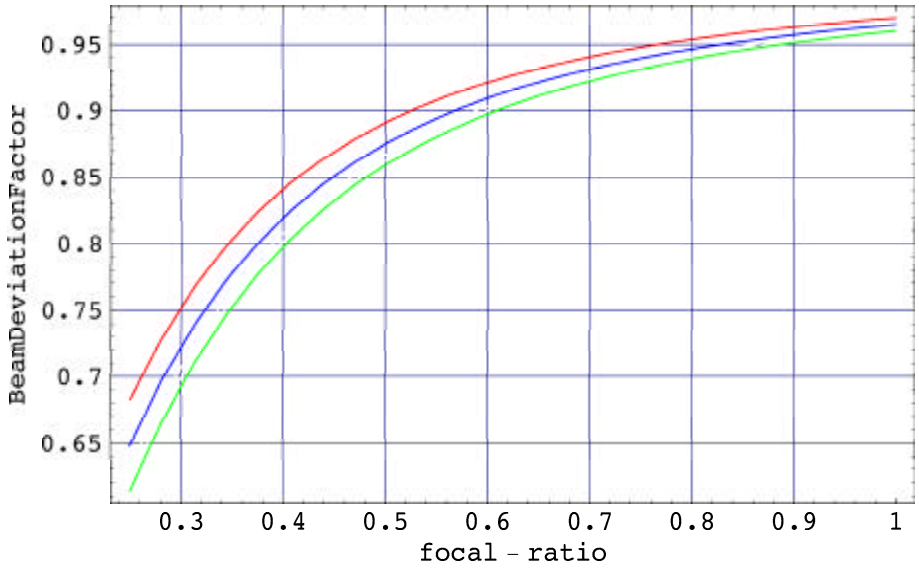

Fig.10a. The BDF for fully tapered (red, upper) and uniform green, (lower curve) illumination as function of the focal ratio of the reflector. The middle curve is for a value of $\tau = 0.25$ (-12 dB) taper.

The BDF approaches one for large f-ratio. For any Cassegrain telescope with an effective f-ratio >> 1 it can safely be taken to be equal to one. Note that a sideways displacement of the subreflector should be treated as a feed movement in the primary focus. The BDF is smallest for uniform illumination. For a tapered illumination, the outer, and more strongly curved, region of the reflector plays a "weaker" role; thus the reflector looks more "flat" and the BDF will increase. The variation of the BDF with illumination is not negligible. Therefore, a good knowledge of the taper is required to accurately estimate the true value of the BDF. This is of importance in the treatment of the influence of systematic (homology) deformations on the pointing correction of the telescope. For instance, the pointing model derived from measurements with a bolometer receiver with a weak taper could cause systematic pointing errors when used with an SIS-receiver with a strongly tapered illumination function. In Fig.10b we show the BDF as function of the illumination taper for several f/D-ratios.

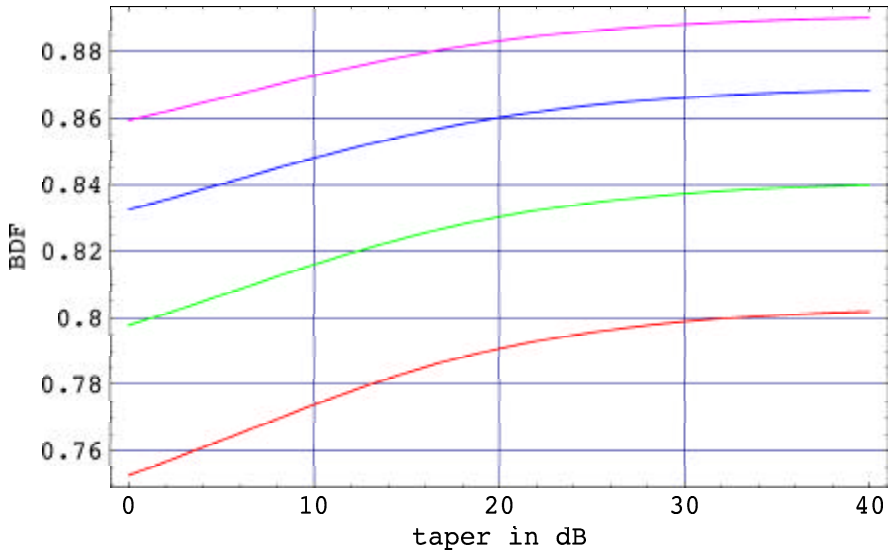

Fig.10b. BDF as function of taper for f/D=0.35-red, 0.4-green, 0.45-blue, 0.5-magenta (bottom to top).

■ 4.2.2. Pointing error

The formulae for the change in pointing direction, as function of the lateral shift and rotation of the feed, main reflector and secondary, are presented below. Translation is reckoned positive in the positive y-direction and rotation is positive when right-handed with respect to the z-axis. Using the symbols K_p and K_s for the Beam Deviation Factor in the primary and secondary focus, respectively, we obtain:

defocus component	**symbol**	**pointing error**	
translation primary	y_p	$-K_p(y_p/f)$	(25a)
rotation primary	ϵ	$(1+K_p)\,\epsilon$	(25b)
translation secondary	y_s	$(y_s/f)\,(K_p - K_s/M)$	(25c)
rotation secondary (vertex)	α	$-\alpha\,(2c/f)\,(K_p+K_s)/(M+1)$	(25d)
rotation secondary (focus)	α	$-\alpha\,(2c/f)\,(K_s/M)$	(25e)
translation feed (in sec. focus)	y_f	$(y_f/f)\,(K_s/M)$	(25f)

The two expressions for the rotation of the secondary apply to rotation about the vertex or the focus of the reflector, respectively. As above, the quantity $2c = f_c$ is the distance between the primary and secondary focus of the Cassegrain system.These formulae are particularly important in the calculation of the pointing shift as function of the elevation angle. The components of translation and rotation are predicted from the Finite Element Analysis (FEA) of the structure. In an optimized design, the different terms will cancel each other partially, leading to a relatively small pointing change with elevation.
The numerical example in Sec.7 uses arbitrary values for the variables of Eq.(25). Translation is in meter, rotation in radian and the output "delpoi" is in arcsecond.

■ 4.2.3. Beam degradation and shift due to lateral defocus

The influence on the beam shape and the gain of the antenna is rather complicated and no simple formulae have been found to describe these in global terms. While the beam moves sideways away from the axis, the gain decreases and the sidelobe level on the side of the antenna axis increases strongly, which is called the Coma-lobe. The sidelobe on the other side decreases. The magnitude of the effects is strongly dependent on the focal ratio; for Cassegrain systems with an effective f-ratio of the order of 10, the effects are weak. This is the great advantage of a Cassegrain for the use of large focal plane arrays.

Curves of gain loss and coma-lobe level are presented in Fig.11 for a primary f-ratio of 0.4. They have been derived from numerical calculations of the beam with lateral defocus present. More data can be found in Ruze (1965) and Baars (1970). Note that the gain and the sidelobe level remain virtually unchanged for a Cassegrain antenna due to its large effective focal length.
We can write for the feed displacement δ_l per HPBW (half power beam width) beam shift

$$\delta_l \;/\; \mathrm{HPBW} = \frac{b}{\mathrm{BDF}} \;\; \frac{f}{D} \;\; \lambda, \qquad (26)$$

where we have used the general expression for the HPBW (see Sect. 3.4, and Fig.7.)

$$\Theta_A \;=\; b\,\frac{\lambda}{D} \qquad \text{(in radian)}, \qquad (27)$$

with b depending on the illumination function with $1.02 < b < 1.27$ between uniform and full parabolic illumination..

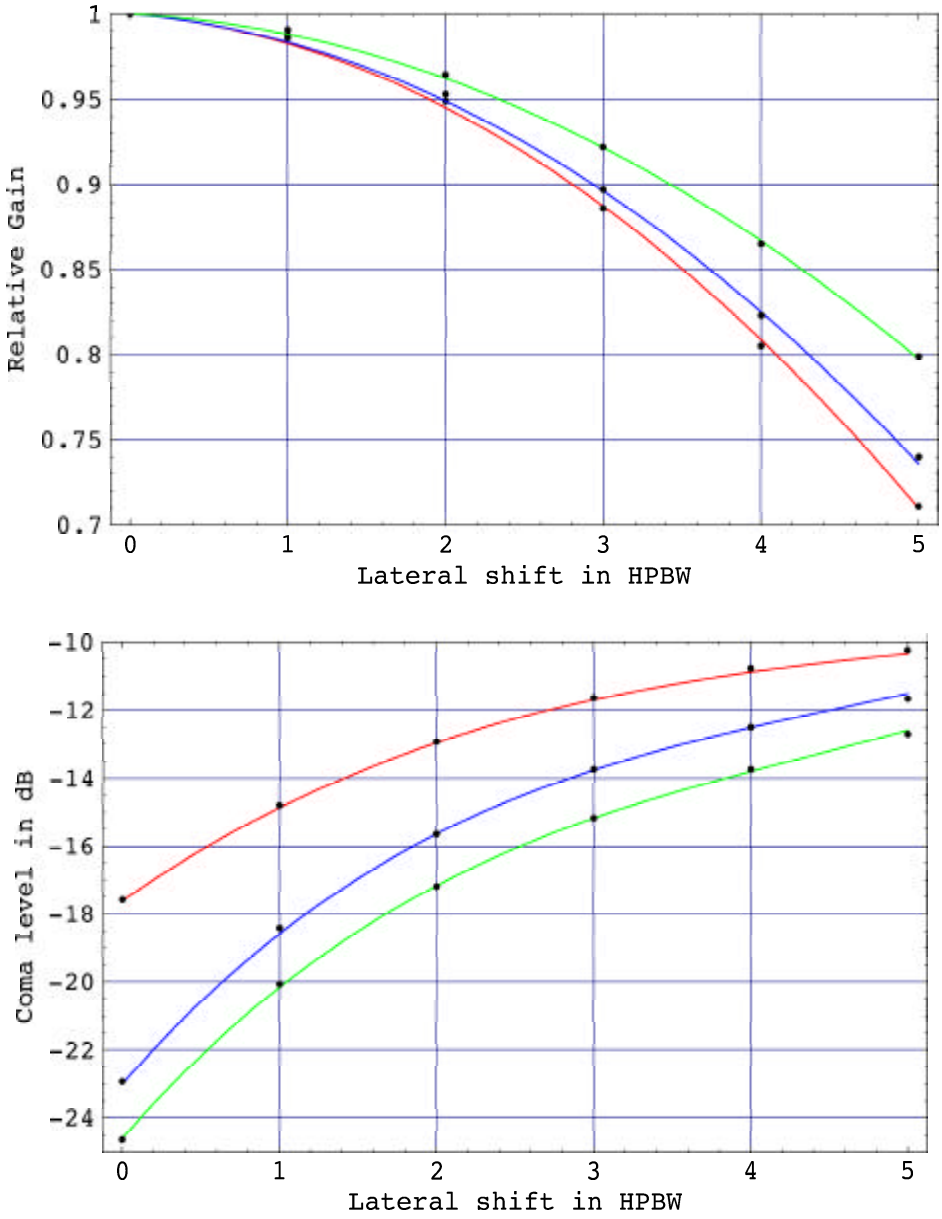

Fig.11. Gain loss and Coma lobe level as function of lateral defocus for uniform (red), -12 dB taper (blue) and parabolic (green) illumination function.

The curves in Fig.11 are the polynomial fits to the computed points at p = 0 to 5 (black points) for an f-ratio of 0.4. They have the following forms:

Illumination		Gain loss function	Coma lobe level (dB)
Uniform	red	1 - 0.0070 p - 0.0102 p^2	-17.6 + 3.2 p - 0.50 p^2 + 0.03 p^3
Taper -12 dB	blue	1 - 0.0073 p - 0.0091 p^2	-23.0 + 5.3 p - 0.95 p^2 + 0.07 p^3
Parabolic	green	1 - 0.0045 p - 0.0072 p^2	-24.6 + 5.3 p - 0.93 p^2 + 0.07 p^3

5. Aperture blocking by secondary reflector and its support

In the common cylindrically symmetric layout of the Cassegrain antenna, the secondary reflector and its support structure (normally a four legged structure, called quadripod) cast a shadow of the incoming wavefront onto the aperture. This is normally called **aperture blocking** or **blockage**. In this section we present the formulae for the calculation of the blocked area and the resulting loss in aperture efficiency. Fig.12 depicts the geometry and defines several variables. We assume a diameter of the central hole in the primary reflector not larger than the diameter of the secondary and a quadripod support structure. This is generally the case.

The shadow on the main reflector, or the aperture, comprises three parts:

1. the central (circular) shadow of the subreflector,

2. "plane wave" shadow of the obstructed area of the infalling wavefront. It is the projection of the quadripod onto the aperture of the main reflector.

3. "spherical wave" shadow, which is caused by the obstruction of the reflected (spherical) waves from the outside section of the reflector on their way to the primary focus. This is the projection of the quadripod onto the aperture as seen from the focus of the primary reflector. It takes the form of approximately a trapezoid growing in width from the point where the legs cross the primary reflector towards the edge of the aperture.

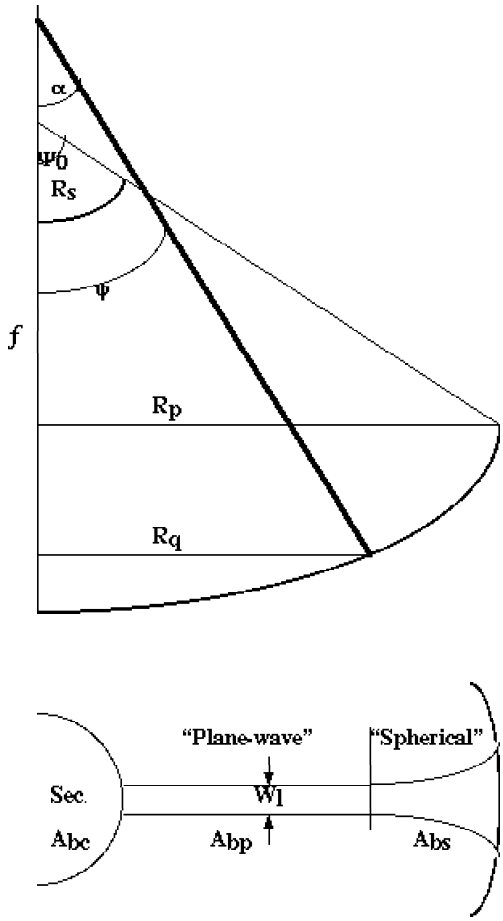

Fig. 12. - Aperture blocking geometry

Inspection of Fig.12 shows that the spherical shadow can easily be the major component of the aperture blocking. To minimize the spherical component, the legs should be directed as far to the outside of the aperture as possible. Often this is a compromise between structural and electro-magnetic considerations. Also, the spherical blocking will be smaller if the quadripod passes farther from the edge of the subreflector. This is the reason for the use of a curved quadripod as for instance in the ALMA antenna, designed by Vertex.

In the following sections we shall define the variables and set up the equations for the blocking components. We follow to a large extent the treatment of E. Maanders, as presented in his doctoral thesis (Maanders, 1978). The *Mathematica* equations are given in Sec.7.

■ 5.1. The variables and equations

We commence with the definition of the variables - see Fig.12.

R_p - radius of primary — D - diameter of primary reflector
R_s - radius of subreflector — d - diameter of subreflector
f - focal length of main reflector
$f^* = f/D$ - focal ratio of primary
$\Psi_0 = 2 \arctan(D/4f)$ - opening half angle of primary
R_q - radius at point of penetration of quadripod through main reflector
α - angle of leg with respect to main reflector axis
$\psi = 2 \arctan(R_q/2f)$ - opening angle to leg penetration point
W_l - width of leg
A_b - total blocked area; — A_{bs} - spherical wave component
A_{bp} - plane wave component, — A_{bc} - central component of blocked areas

Here follow the equations for the different blocking components:

1. Central obstruction due to subreflector

$$A_{bc} = \pi R_s^2 \tag{28a}$$

2. Plane wave shadow area (assumes four legs)

$$A_{bp} = 4 W_l (R_q - R_s) \tag{28b}$$

3. Spherical wave shadow area (4 legs)

$$A_{bs} = \frac{4 W_l}{AB}\left[\frac{R_p{}^2 - R_q{}^2}{2} - (R_p - R_q) f \tan(\alpha) + \frac{\tan(\alpha)}{12 f}(R_p{}^3 - R_q{}^3)\right], \tag{28c}$$

where $AB = R_q[1 - \tan(\alpha)/\tan(\psi)]$

These formulae are valid for a uniform illumination of the aperture.

For a tapered illumination function we assume a quadratic illumination function with a taper of -11 dB at the aperture edge. We obtain the following **correction terms** to be **subtracted** from Eqs.(28b) and (28c) above, respectively:

$$A_{\mathrm{bp}}(t) = \frac{4\,W_l{*}0.7}{3\,R_p{}^2}\,(R_q{}^3 - R_s{}^3) \tag{28d}$$

$$A_{\mathrm{bs}}(t) = \frac{4\,W_l{*}0.7}{\mathrm{AB}{*}R_p{}^2}\left[\frac{R_p{}^4 - R_q{}^4}{4} - f\,\tan(\alpha)\,\frac{R_p{}^3 - R_q{}^3}{3} + \frac{\tan(\alpha)}{20\,f}\,(R_p{}^5 - R_q{}^5)\right]. \tag{28e}$$

This formulation assumes that the quadripod just skims the edge of the subreflector. Without this restriction, the following **alternative formula for the spherical blocking** can be derived, leading to only very small changes (~1%) in the numerical outcome of the spherical blocking term. The tapered corrections of Eqs.(28d,28c) can be applied to this formula too.

$$A_{\mathrm{bs}}(\mathrm{alt}) = 2\;W_l(R_p - R_q)\left(1 + \frac{R_p}{\sin\Psi_0}\Big/\left(\frac{\sin\alpha}{\sin(\Psi_0-\alpha)}\left(\frac{R_q{}^2}{4\,f} + \frac{R_q}{\tan\alpha} - f\right)\right)\right). \tag{28f}$$

Note that the effect of the blocking is expressed as a shadow, projected onto the **aperture** of the reflector. Hence, the blocking percentage is obtained by dividing this number by the area of the aperture A_r, not the physical area of the curved reflector.

The *Mathematica* expressions for the computation of the blocking, together with the necessary input parameters, are to be found in Section 7.5 below. The numerical values there are taken from the ALMA prototype antenna design by EIE. They can be replaced by any others before running the expressions for the blocking.

■ 5.2. Gain loss due to blockage

The loss of gain caused by the blocking, which we call here the **blocking efficiency** η_b, is given by the following expression:

$$\eta_b = (1 - A_b / A_r)^2 \approx 1 - 2\,(A_b / A_r), \tag{29}$$

the approximation being accurate to 1 percent or better if $A_b / A_r \ll 0.1$, which will normally be the case. The "double" effect of the blocking can be understood physically by considering that the blocking causes:

a) a decrease in the reflector area exposed to the incoming wavefront, and
b) a reduction of the incoming energy which will be available for reflection to the focus.

A further result of the blocking is the increase of the sidelobe level due to the discontinuous aperture distribution and the scattering of the incoming wavefront by the blocking structures. A central obscuration with a diameter of 10% of the aperture diameter increases the first sidelobe by about 1.5 - 2 dB.
A particularly interesting effect is the scattering of the obliquely infalling wavefront on the quadripod. This causes a *scattering cone* with a top angle determined by the angle α, i.e. typically some 40 degrees from boresight. The intensity of this "cone" is dependent on the width of the quadripod and is strongest if the width is of the order of the wavelength. Near the beam axis one sees an increased sidelobe level along the projection of the quadripod. For an example of these features see Hartsuijker et al. (1972).

6. Deviations from the prescribed reflector shape

■ 6.1. Random surface deviation

Every antenna will suffer from fabrication errors and from deformations caused by gravity, wind and thermal effects. These will result in more or less randomly distributed deviations of the reflector surface from the theoretical shape. The influence of such random errors has been treated by Ruze (1966) and often these errors are called "Ruze error". It should be understood that the analysis of Ruze is strictly valid only for errors which are small with respect to the wavelength, are randomly distributed over the reflector with mean-square value $< \epsilon^2 >$ and exhibit a "correlation length" c which is much smaller than the reflector diameter and much larger than the wavelength. In practice, it has been determined that these restrictions need not be satisfied rigorously in order to give satisfactory results. The physical effect of the random deviations is to remove power from the main beam and distribute this in a wide "scatter pattern", the half power width of which is determined by the correlation length. Thus the total antenna beam can be written as the sum of the diffraction pattern and the error beam in the following form:

$$f(\theta) = f_D(\theta) + f_E(\theta, \epsilon)$$

Without going through the analysis (see e.g. Ruze (1966) and Baars (1973)), the relative aperture efficiency can be written as

$$\eta_e = \frac{\eta_A}{\eta_{A0}} = \exp(-\sigma^2) + \frac{1}{\eta_{A0}} \left(\frac{c}{D}\right)^2 \{1 - \exp(-\sigma^2)\}, \qquad (30)$$

where η_{A0} is the aperture efficiency of the perfect reflector, c and D the correlation length and reflector diameter, respectively, with c<<D, and σ the root-mean-square phase fluctuation over the aperture, given by the expression

$$\sigma = \frac{4\pi}{\lambda} \sqrt{< \epsilon >^2} \equiv \frac{4\pi\epsilon}{\lambda}. \qquad (31)$$

The actual surface deviations ϵ_n are mostly calculated or measured *normally* to the reflector surface. However, the phase error is proportional to the pathlength change and hence ϵ is the component of this deviation ϵ_n parallel to the antenna axis. The relationship between the two quantities is dependent on the focal ratio and is given by

$$\epsilon = \epsilon_n \cos\left(\frac{\psi}{2}\right) \equiv \frac{\epsilon_n}{\sqrt{1+(r/2f)^2}}. \qquad (32)$$

Thus the errors towards the edge of the reflector have a smaller influence on the overall rms error. In practice, in order to calculate the expected gain loss caused by the random surface deviations, one can also weigh the measured errors by the illumination function over the aperture, again diminishing the effect of the outside regions of the reflector (see e.g. Greve and Hooghoudt, 1981).

The first term in Eq.(30) is the usual form of the "Ruze" loss caused by small random surface errors. The second term is the maximum level of the "error beam", which is both dependent on the correlation length and the phase error. Normally, the second term is negligible for the resulting loss in antenna efficiency, but for relatively large phase errors and large correlation length it can be significant. In any case, it is of considerable significance for the observation of extended sources, because the error beam will be "filled" by the extended structure and lead to overestimation of the flux density. The peak level of the error beam with respect to the peak of the main beam is

$$\frac{f_E(0)}{f_D(0)} = \frac{1}{\eta_{A0}} \left(\frac{c}{D}\right)^2 \{\exp(\sigma^2) - 1\}, \qquad (33)$$

while the half power width of the gaussian shaped error pattern is given by

$$\theta_E = 2\sqrt{\ln 2}\left(\frac{2\lambda}{\pi c}\right) = 1.06\ \frac{\lambda}{c}. \qquad (34)$$

The ratio of the power scattered into the error beam to that in the main beam can be found from these equations. The beam solid angle of a gaussian pattern profile is given by the simple relation

$\Omega_b = 1.133\ \Theta_A{}^2$, where Θ_A is the half power beam width.

Approximating the main beam by a gaussian too, we obtain for the **ratio of the power in error to main beam**, using Eqs. (33), (34) and Eq. (27) with b=1.2 (a typical value for practical tapers, see Fig. 7),

$$\frac{P_E}{P_M} = \frac{f_E(0)\,\Omega_E}{f_D(0)\,\Omega_M} \approx 1.1\,\{\exp(\sigma^2) - 1\}. \qquad (35)$$

Note that this quantity is not dependent on the correlation length; it is solely determined by the rms surface error. From Eqs.(33) and (34) it is clear that a smaller correlation length will lead to a wider error pattern with a smaller peak level. For the observation of relatively small, be it extended, sources this will normally be preferable. However, even the very low error beam level, extending over a large solid angle can hamper observations of widely distributed radiation, as for instance the Galactic neutral hydrogen.

Finally, an interesting result can be obtained from a measurement of the beam efficiency on a point source (η_B) and on an extended source (η_{Bs}) of a known size (θ_S) larger than the main beam and smaller than the error beam (Baars, 1973). The correlation length can be derived from those two measurements as

$$c = \frac{4\lambda}{\pi\theta_S}\left\{-\ln\left(\frac{\eta_{B0}-\eta_{Bs}}{\eta_{B0}-\eta_B}\right)\right\}^{0.5}, \qquad (36)$$

where η_{B0} is the beam efficiency of the perfect reflector.

Often, the correlation length is determined by the size of the individual panels, making up the reflector. Thus values of D/c will typically lie between 6 and 20, depending on the number of panel rings.

■ 6.2. The numerical results in *Mathematica*

We begin with Eq.(30) for the gain loss due to random errors, plotting the relative aperture efficiency, also called the surface error efficiency η_e, as function of wavelength for several error values. We use D/c = 10 for this example; further we assume that $1/\eta_{A0} = 1.4$..

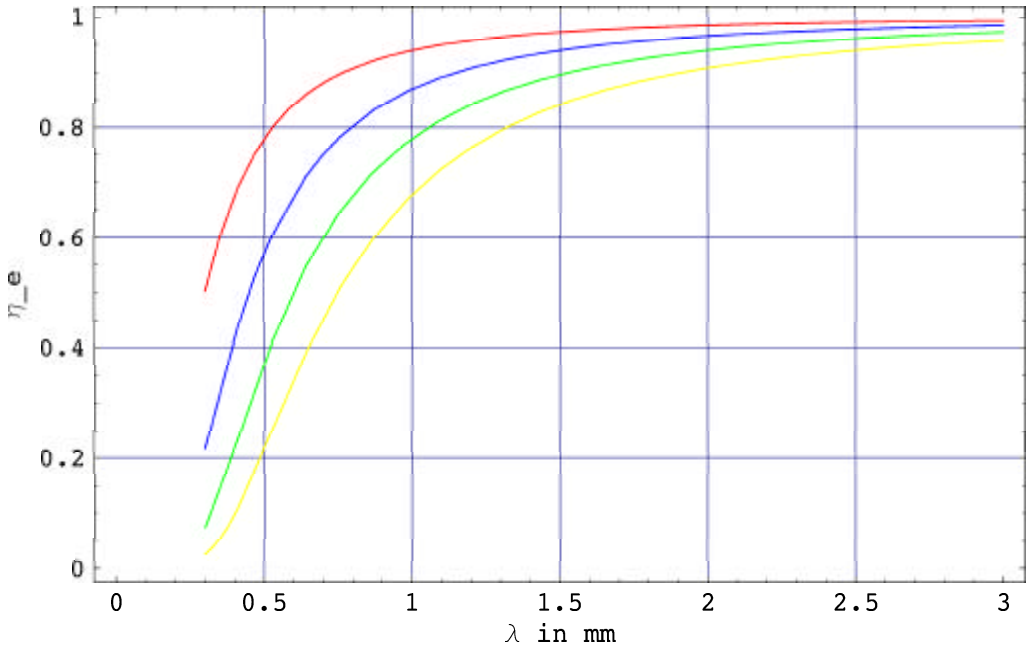

Fig.13. Surface error efficiency η_e as function of wavelength (λ in mm) for four values of the rms error ϵ=20,30,40 and 50 μm from top to bottom graph. Here D/c=10; larger values of this ratio make essentially no difference.

The following plot shows the same relation, but now as function of the rms error with the wavelength as parameter. For simplicity, we have dropped the insignificant second term in Eq.(30) from the computation.

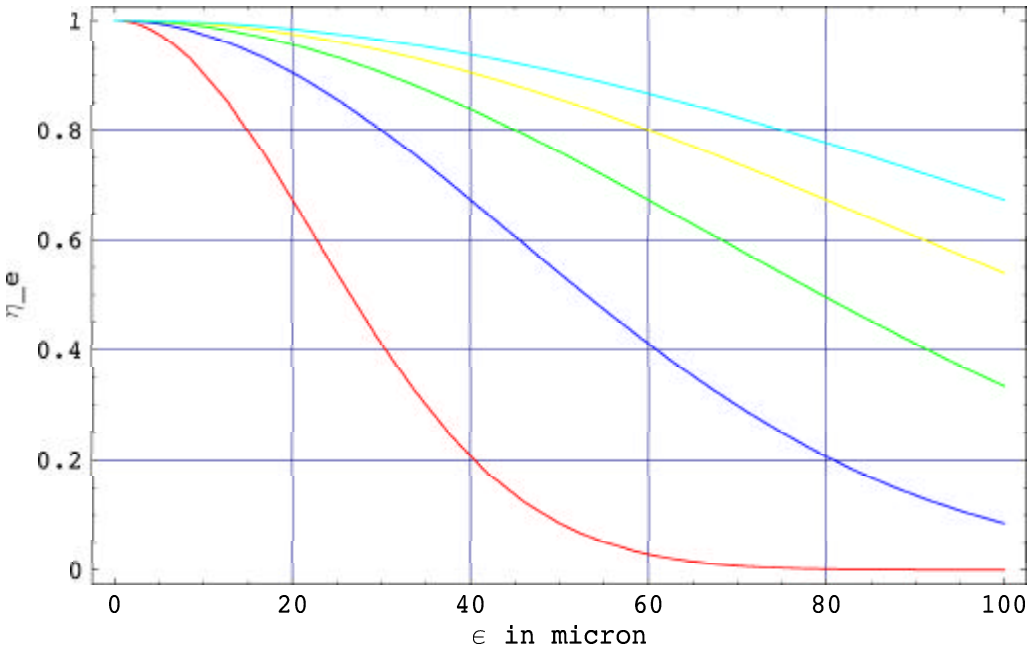

Fig.14. Surface error efficiency η_e as function of the rms error ϵ (in micrometers) for 5 values of the wavelength, λ= 0.4, 0.8, 1.2, 1.6 and 2.0 mm from bottom to top.

A single curve of the surface error efficiency as function of the ratio $\delta = \epsilon/\lambda$ is shown in Fig.15.

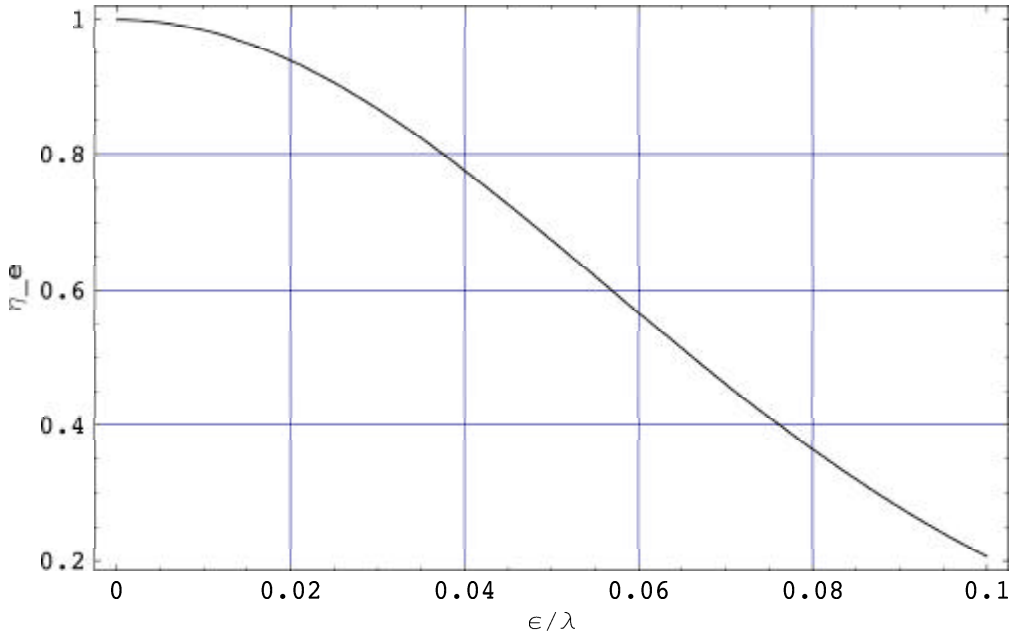

Fig.15. Surface error efficiency η_e as function of the ratio rms error to wavelength.

Here is a set of curves, representing Eq.(33), of the level of the error pattern $f_E(0)$ with respect to that of the (weakened) main beam $f_D(0)$ as function of ϵ/λ and for a number of values of the ratio $c^* = c/D$.

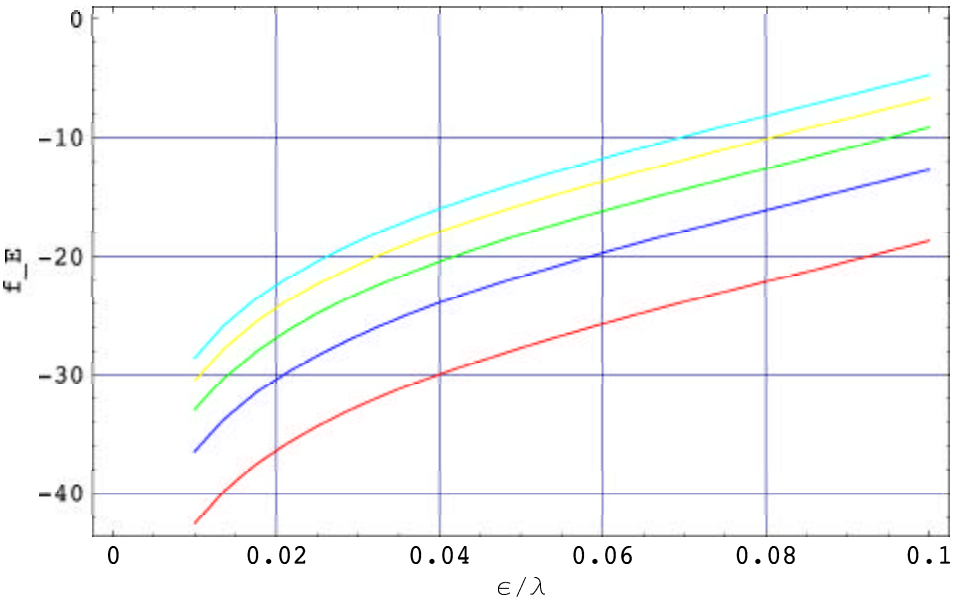

Fig.16. The level of the error beam (in dB) with respect to the main beam as function of the ratio rms error to wavelength (ϵ/λ); parameter is the ratio c/D = 0.05 to 0.25 in steps of 0.05 from bottom.

From Fig.16 one sees that for an rms error of less than λ/20 and a correlation length smaller than D/6 the error pattern level stays below approximately -20 dB, i.e. comparable with the normal sidelobe level of the main diffraction pattern. In conclusion, the relation of Eq.(35), showing the ratio of the power in the error pattern to that in the main beam is depicted in Fig.17. When the rms surface error approaches one twentieth of a wavelength, about thirty percent of the received power is distributed to the error pattern.

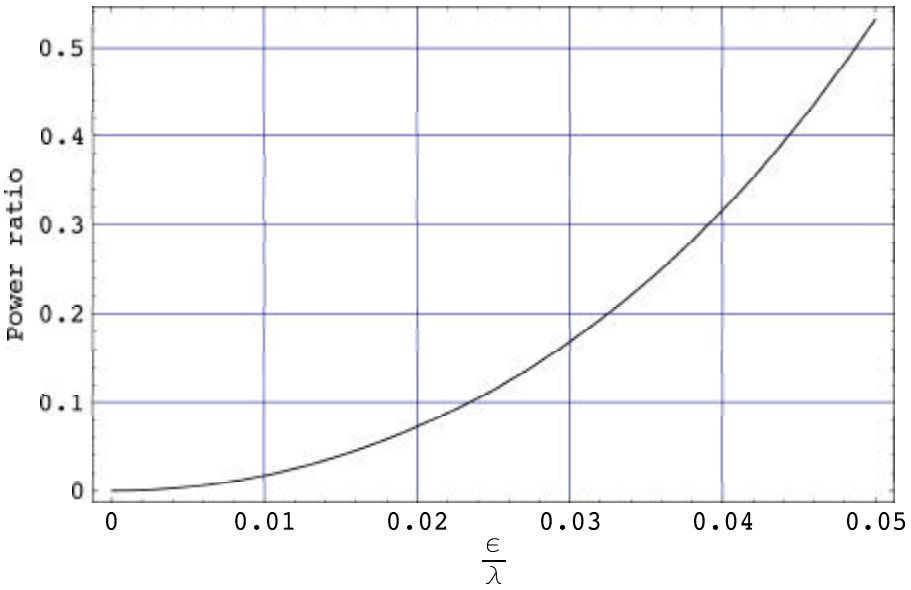

Fig. 17. The ratio of the power in the error pattern to that in the main beam as function of the surface error in units of the wavelength.

7. The *Mathematica* expressions with numerical examples

Here we collect the *Mathematica* expressions used in the text and as source for the Figures. As an example we supply these with numerical values pertaining to the ALMA Prototype antenna. When running this section within *Mathematica* these input values can be edited and all expressions run to provide an amended set of curves. Note that *Mathematica* treats angels in radians.

7.1. The **geometrical input data** and basic parameter calculations of the ALMA antenna.

```
Dp = 12.0
F = 4.8
m = 20.
d = 0.75
Ψ0 = 2 ArcTan[Dp / (4 F)] (180 / π)
Φ0 = 2 ArcTan[Dp / (4 m F)] (180 / π)
e = (m + 1) / (m - 1)
m = (e + 1) / (e - 1)
c = (d / 4) (Cot[Ψ0 π / 180] + Cot[Φ0 π / 180])
fc = 2 c
l = c (e - 1) / e
```

7.2. Here are the formulae connected to the calculation of the **illumination efficiency** as depicted in Figs. 2 to 5. These are Eq.10, Eqs.12+14 and Eqs. 13+15 and their plots.

```
Plot[20 Log[10, 1 + (1 / (4 fr))^2], {fr, .25, 2}, GridLines → Automatic,
 FrameLabel -> {"f/D", "free-space taper (dB)"}, Frame -> True]
```

```
ig = Exp[-1.2664 r^2]
ip = 1 - (1 - 0.282) r^2
Plot[{ig, ip}, {r, 0, 1}, Frame -> True,
 GridLines -> Automatic, FrameLabel -> {Radius, Illum_Func},
 PlotStyle -> {{RGBColor[1, 0, 0]}, {RGBColor[0, 0, 1]}}]
```

$$jg = \frac{2\,(1 - \text{Exp}[-(T\,\text{Log}[10]/20)])^2}{(T\,\text{Log}[10]/20)\,(1 - \text{Exp}[-(T\,\text{Log}[10]/10)])}$$

$$jp = \frac{3\,(1 + 10^{(-T/20)})^2}{4\,(1 + 10^{(-T/20)} + 10^{(-T/10)})}$$

```
Plot[{jg, jp}, {T, 0, 30}, Frame → True, GridLines → Automatic,
 PlotStyle → {{RGBColor[1, 0, 0]}, {RGBColor[0, 0, 1]}},
 FrameLabel -> {"Taper in dB", "Illum_Eff"}]
```

The following set of Bessel functions from Eq.17 delivers the **radiation power pattern** of a circular aperture for taper values between 1 and 0 and plots Fig.6.
We omit the simple curve fittings of Figs. 7 and 8, Eqs. 18 and 19.

```
τ = 1
g10 = (2 τ BesselJ[1, u] / u + 4 (1 - τ) BesselJ[2, u] / u^2)^2
τ = 0.8
g08 = (1.111 (2 τ BesselJ[1, u] / u + 4 (1 - τ) BesselJ[2, u] / u^2))^2
τ = 0.6
g06 = (1.25 (2 τ BesselJ[1, u] / u + 4 (1 - τ) BesselJ[2, u] / u^2))^2
τ = 0.4
g04 = (1.429 (2 τ BesselJ[1, u] / u + 4 (1 - τ) BesselJ[2, u] / u^2))^2
τ = 0.2
g02 = (1.667 (2 τ BesselJ[1, u] / u + 4 (1 - τ) BesselJ[2, u] / u^2))^2
τ = 0
g00 = 4 (2 τ BesselJ[1, u] / u + 4 (1 - τ) BesselJ[2, u] / u^2)^2
g = {g10, g08, g06, g04, g02, g00}
Plot[Evaluate[g], {u, 0, 5}, Frame -> True,
 GridLines -> Automatic, FrameLabel -> {"u", "g(u)"}]
```

7.3. The **depth of focus** of Eq.22 and the **gain formula with axial defocusing (Eq. 23) with plot of** Fig.9 follow.

```
df = 1 + (1 - Cos[Ψ0 π / 180]) / (1 - Cos[Φ0 π / 180])

β = (2 π δ) (2 - Cos[Φ0 π / 180] - Cos[Ψ0 π / 180])
Plot[Evaluate[Table[τ^2 * (Sin[β / 2] / (β / 2))^2 + (1 - τ)^2 *
      ((Sin[β / 2] / (β / 2))^4 + (4 / β^2) (Sin[β] / β - 1)^2), {τ, 0, 1}]],
 {δ, 0, 2}, FrameLabel -> {"δ/λ", "Gain"}, Frame -> True,
 GridLines -> Automatic,
 PlotStyle -> {{RGBColor[1, 0, 0]}, {RGBColor[0, 0, 1]}}]
```

7.4 The **pointing formula** for the defocus components of (Eq. 25) is called "delpoi" with arbitrary input values below. The **Beam Deviation Factor** (BDF) formula of Eq.24 is written in the two forms for production of Figs..10a and 10b.

```
Kp = 0.82
Ks = 1.0
c = 3.0885
ϵ = .00001
yp = 0.001
ys = 0.001
α = -0.00002
yf = 0

delpoi = (180 * 3600 / Pi) (-Kp (yp / F) + (1 + Kp) ϵ +
     (ys / F) (Kp - Ks / m) - α (2 c / F) (Kp + Ks) / (m + 1) + (yf / F) (Ks / m))
```

$$\text{BDFnum} = \int_0^1 \frac{(1 - (1 - \tau)\, r^2)\, r^3}{1 + \left(\frac{r}{4f}\right)^2}\, dr$$

$$\text{BDFdenom} = \int_0^1 (1 - (1 - \tau)\, r^2)\, r^3\, dr$$

```
Plot[Evaluate[Table[BDFnum / BDFdenom, {τ, 0, 1, .25}],
  {f, 0.25, 1}, Frame → True, GridLines → Automatic,
  FrameLabel → {focal - ratio, BeamDeviationFactor},
  PlotStyle → {{RGBColor[1, 0, 0]}, {RGBColor[0, 0, 1]},
    {RGBColor[1, 1, 1]}, {RGBColor[1, 1, 1]}, {RGBColor[0, 1, 0]}}]]
```

$$-4\,(-f^2 - 32 f^4 - f^2 \tau + 32 f^4 \tau - 32 f^4 \text{Log}[16 f^2] - 512 f^6 \text{Log}[16 f^2] + 512 f^6 \tau \text{Log}[16 f^2] + 32 f^4 \text{Log}[1 + 16 f^2] + 512 f^6 \text{Log}[1 + 16 f^2] - 512 f^6 \tau \text{Log}[1 + 16 f^2])$$

$$\frac{1}{12} + \frac{\tau}{6}$$

$$\text{num} = \int_0^1 \frac{(1 - (1 - 10^{-t/20})\, r^2)\, r^3}{1 + \left(\frac{r}{4F}\right)^2}\, dr$$

$$\text{den} = \int_0^1 (1 - (1 - 10^{-t/20})\, r^2)\, r^3\, dr$$

```
BDF = num / den

Plot[Evaluate[Table[BDF, {F, .35, .5, .05}],
  {t, 0, 40}, Frame -> True, GridLines → Automatic,
  FrameLabel → {"taper in dB", "BDF"},
  PlotStyle -> {{RGBColor[1, 0, 0]}, {RGBColor[0, 1, 0]},
    {RGBColor[0, 0, 1]}, {RGBColor[1, 0, 1]}}]]
```

For curiosity, we can also illustrate the above expression in one "3-dimensional" plot as shown below. The taper and f/D-ratio axes run in the "horizontal" plane.

```
Plot3D[Evaluate[BDF, {F, .25, 1}, {t, 0, 30},
  ViewPoint → {-2, -2, 0}, BoxRatios → {1, 1, .75},
  AxesLabel → {"f/D-ratio", "Taper(dB)", "BDF"}, Mesh → True]]
```

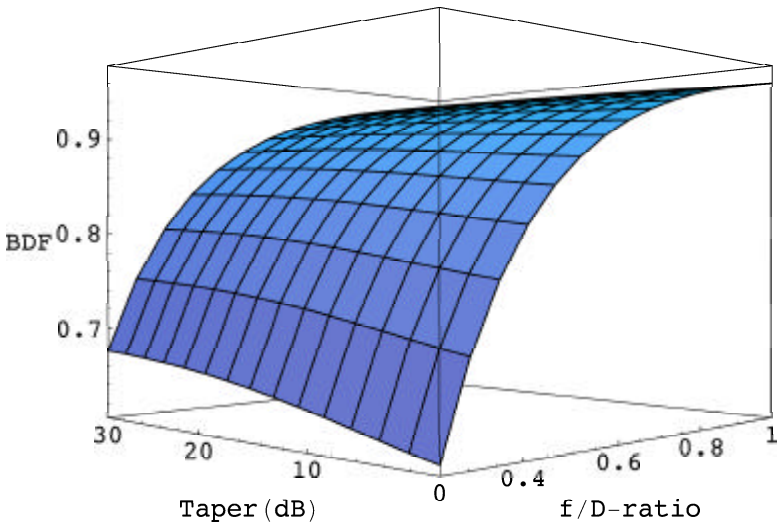

7.5. We come now to the **blocking formulae** of Sec.5. First we list the antenna's blocking geometry parameters, after which the formulae for the different blocking contributions are given, before we finish with the overall blocking and percentage blocking expressions (Eqs. 28 a-f).

```
Rp = 6.0
Rs = 0.375
Rq = 4.11
F = 4.8
Wl = 0.06
α = 42.89 π / 180
Ψ0 = 2 ArcTan[Rp / (2 F)]
ψ = 2 ArcTan[Rq / (2 F)]
```

$$Ar = \pi\, Rp^2$$
$$As = \pi\, Rs^2$$
$$Abp_u = 4\, Wl\, (Rq - Rs)$$
$$Abp_t = \frac{4\, Wl\, 0.7}{3\, Rp^2}\, (Rq^3 - Rs^3)$$
$$AB = Rq\, (1 - Tan[\alpha] / Tan[\psi])$$
$$Abs_u = \frac{4\, Wl}{AB}\left(\frac{Rp^2 - Rq^2}{2} - (Rp - Rq)\, F\, Tan[\alpha] + \frac{Tan[\alpha]}{12\, F}\, (Rp^3 - Rq^3)\right)$$
$$Abs_t = \frac{4\, Wl\, 0.7}{AB\, Rp^2}\left(\frac{(Rp^4 - Rq^4)}{4} - F\, Tan[\alpha]\, \frac{(Rp^3 - Rq^3)}{3} + \frac{Tan[\alpha]}{20\, F}\, (Rp^5 - Rq^5)\right)$$
$$Abs_a = 2\, Wl\, (Rp - Rq)\left(1 + \frac{Rp}{Sin[\Psi_0]} \Big/ \left(\frac{Sin[\alpha]}{Sin[\Psi_0 - \alpha]}\left(\frac{Rq^2}{4\, F} + \frac{Rq}{Tan[\alpha]} - F\right)\right)\right)$$

$$Ab = As + Abp_u + Abs_u$$
$$BlPer = 100\,\% / Ar$$

$$Ab_a = As + Abp_u + Abs_a$$
$$BlPer = 100\,\% / Ar$$

$$Ab_t = Ab - Abp_t - Abs_t$$
$$BlPer_t = 100\,\% / Ar$$

$$Ab_{ta} = Ab_a - Abp_t - Abs_t$$
$$BlPer_{at} = 100\,\% / Ar$$

7.6. The effects of **random surface errors** are presented here. Based on Eq.30, the first three plot expressions provide Figs. 13-15, while the following two treat the error pattern level of Eq.33/Fig.16 and Eq.35/Fig.17. These expressions are self-contained and the **range of the variables can be varied at will within the formulae.**

```
c* = 0.1
 Plot,
 Evaluate[Table[(Exp[-(4 π ϵ/(100 * λ))^2] + 1.4 (c*)^2 (1 - Exp[-(4 π ϵ/(100 * λ))^2])),
   {ϵ, 2, 5, 1}]], {λ, .3, 3}, FrameLabel -> {"λ in mm", "η_e"},
 Frame -> True, GridLines -> Automatic,
 PlotStyle → {{RGBColor[1, 0, 0]}, {RGBColor[0, 0, 1]},
   {RGBColor[0, 1, 0]}, {RGBColor[1, 1, 0]}}]

Plot[Evaluate[Table[Exp[-(4 * π * ϵ/(1000 * λ))^2], {λ, .4, 2, .4}]],
 {ϵ, 0, 100}, FrameLabel -> {"ϵ in micron", "η_e"},
 Frame -> True, GridLines -> Automatic,
 PlotStyle → {{RGBColor[1, 0, 0]}, {RGBColor[0, 0, 1]},
   {RGBColor[0, 1, 0]}, {RGBColor[1, 1, 0]}, {RGBColor[0, 1, 1]}}]
```

```
Plot[Exp[-(4 π δ)^2], {δ, 0, 0.1}, FrameLabel -> {"ϵ/λ", "η_e"},
 Frame -> True, GridLines -> Automatic]

Plot[Evaluate[Table[10 Log[10, 1.4 * c*^2 * (Exp[(4 π δ)^2] - 1)],
   {c*, 0.05, 0.25, 0.05}]], {δ, .01, 0.1}, Frame -> True,
 GridLines -> Automatic, FrameLabel -> {"ϵ/λ", "f_E"},
 PlotStyle → {{RGBColor[1, 0, 0]}, {RGBColor[0, 0, 1]},
   {RGBColor[0, 1, 0]}, {RGBColor[1, 1, 0]}, {RGBColor[0, 1, 1]}}]

Plot[1.1 (Exp[(4 π δ)^2] - 1), {δ, 0, .05}, GridLines -> Automatic,
 Frame -> True, FrameLabel -> {"ϵ/λ", "Power ratio"}]
```

We add some 3D-plots here as illustrations. First the scatter efficiency against ϵ/λ and C, the correlation ratio (to D). Then the error beam level, in dB below the peak of the diffraction beam against ϵ/λ and the correlation ratio.

```
p1 = Plot3D[
  Evaluate[Exp[-(4 π δ)^2] + 1.4 (C)^2 (1 - Exp[-(4 π δ)^2]), {δ, 0, .1},
   {C, .025, .3}, ViewPoint → {2, -2, 0}, BoxRatios → {1, 1, .75},
   DisplayFunction → Identity, AxesLabel → {"ϵ/λ", "CorLen", "η"}]]

p2 = Plot3D[Evaluate[10 Log[10, 1.4 * C^2 * (Exp[(4 π δ)^2] - 1)],
   {C, 0.025, 0.3}, {δ, .01, 0.1}, ViewPoint → {-2, -2, 1},
   BoxRatios → {1, 1, .8}, DisplayFunction → Identity,
   AxesLabel → {"CorLen", "ϵ/λ", "f_E"}]]

Show[GraphicsArray[{p1, p2}]]
```

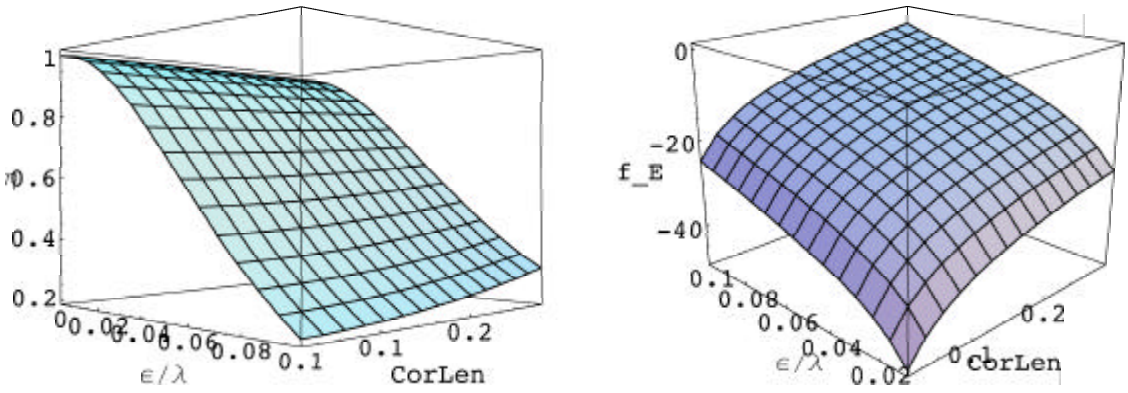

8. References

Baars, J.W.M., "Characteristics of the Paraboloidal Reflector Antenna", NRAO - EDIR 57, Aug. 1966
Baars, J.W.M., "Dual-beam parabolic antennae in radio astronomy", Dissertation Tech. Univ. Delft, 1970
Baars, J.W.M., "The Measurement of large antennas with cosmic radio sources", IEEE Trans. **AP-21**, 171, 1973
Greve, A. & Hooghoudt, B.G., "Quality evaluation of radio reflector surfaces", Astron Astrophys **93**, 76, 1981
Hartsuijker, A.P., Baars, Drenth & Gelato-Volders, "Interferometric measurement of radiation pattern...", IEEE Trans. **AP-20**, 166, 1972
Jahke-Emde, "Tables of Functions", p.180ff, Dover Books
Kraus, J.D., "Radio Astronomy", 2nd Edition,Cygnus-Quasar Books, 1982
Maanders, E. Dissertation Univ. Ghent, 1978
Mangum & Cheng, "Feed leg blockage and ground radiation pickup for Cassegrain Antennas", MMA-Memo No. 197, Feb. 1998
Ruze, J., "Lateral feed displacement in a Paraboloid", IEEE Trans. Antennas & Prop. **AP-13**, 660, 1965
Ruze, J., "Antenna Tolerance theory - A review" Proc IEEE **54**, 633, 1966
Silver, S., "Microwave antenna theory and design:, MIT Rad. Lab. Series No. 12, 1949

Acknowledgement. I thank Jeff Mangum for a critical reading of the manuscript and a number of suggestions for improvement of the text.